AGU100 ADVANCING EARTH AND SPACE SCIENCE

Geochemistry, Geophysics, Geosystems

RESEARCH ARTICLE
10.1029/2018GC007696

Key Points:
- Vertical fractures dominate the permeability structure of the transition between dikes and lavas at IODP Hole 1256D
- Diking opens new vertical pathways for hydrothermal circulation outside the neovolcanic zone
- Crustal permeability is reduced by 1–2 orders of magnitude by vein filling

Supporting Information:
- Supporting Information S1
- Data Set S1
- Data Set S2
- Data Set S3
- Data Set S4

Correspondence to:
L. A. Gilbert,
lgilbert@williams.edu

Citation:
Gilbert, L. A., Crispini, L., Tartarotti, P., & Bona, M. L. (2018). Permeability structure of the lava-dike transition of 15-Myr-old oceanic crust formed at the East Pacific rise. *Geochemistry, Geophysics, Geosystems*, *19*, 3555–3569. https://doi.org/10.1029/2018GC007696

Received 24 MAY 2018
Accepted 25 AUG 2018
Accepted article online 3 SEP 2018
Published online 28 SEP 2018

Permeability Structure of the Lava-Dike Transition of 15-Myr-Old Oceanic Crust Formed at the East Pacific Rise

L. A. Gilbert[1], L. Crispini[2], P. Tartarotti[3], and M. L. Bona[1]

[1]Geoscience and Marine Science at Williams-Mystic, Williams College, Williamstown, MA, USA, [2]Dipartimento di Scienze della Terra, dell'Ambiente e della Vita, Università degli Studi di Genova, Genoa, Italy, [3]Dipartimento di Scienze della Terra, Università degli Studi di Milano, Milan, Italy

Abstract The permeability structure of oceanic crust controls both the spatial and temporal extent of hydrothermal circulation, but the detailed geometry of fractures in seafloor rocks is not well known. We apply an equivalent channel model to veins, joints, faults, and breccias preserved in recovered cores from ODP-IODP Hole 1256D to calculate paleo-permeability. In the ~250-m transition between dikes and lavas, paleo-permeability is 10^{-13}~10^{-14} m^2 with narrow zones of $>10^{-9}$ m^2 that presumably act as conduits for the largest volume of fluids. Most of these high-permeability zones are oriented vertically as a result of diking events into a significant thickness of lavas outside of the neovolcanic zone. After an increase in permeability due to off-axis diking events, fluid temperatures drop, pathways are sealed, and the permeability of the upper oceanic crust drops significantly.

1. Introduction

The lava-dike transition in young oceanic crust is an important zone for understanding the geological construction, as well as the geophysical evolution and alteration history, of the seafloor. The lava-dike transition is both a lithological boundary between intrusive and extrusive basalts and an interval of significant physical gradients (Becker et al., 2004; Carlson, 2010; Gilbert & Bona, 2016; Karson, Klein, et al., 2002; Seher et al., 2010). Significant seismic velocity gradients in oceanic crust (Fox et al., 1973; Houtz & Ewing, 1976) have been associated with the lithological change from dikes to lavas (Christeson et al., 2010, 2012; Honnorez et al., 1985; Hooft et al., 1996; Karson, Klein, et al., 2002). Seismic velocity gradients have also been attributed to changes in porosity and alteration observed in the transition between dikes and lavas (e.g., Carlson, 2014; Gilbert & Salisbury, 2011; Gillis, 1995; Wilkens et al., 1991), and these changes are related to changes in permeability (Carlson, 2014).

The lava-dike transition is commonly characterized by intense rock fracturing and the distribution and orientation of fractures is particularly important for controlling hydrothermal circulation (Karson et al., 2002). High concentrations of fractures or a damage zone can act to channelize fluid circulation more acutely than weakly fractured rocks (Tsang & Neretnieks, 1998). For example, in Deep Sea Drilling Project and Ocean Drilling Program (DSDP-ODP) Hole 504B (Costa Rica Rift, Nazca Plate), the lava-dike transition is highly fractured (Pezard et al., 1997), and contains stockwork-like sulfide mineralization, breccias, and veins (Anderson et al., 1985; Honnorez et al., 1985). In particular, steeply dipping permeable features facilitate vigorous hydrothermal circulation above a heat source (Rowland & Sibson, 2004), although horizontal or subhorizontal conduits are necessary for lateral circulation (Fisher, 1998).

Vertical and subvertical fractures and faults in oceanic crust are caused by a number of processes. Contractional cooling effects (e.g., Lister, 1974), the regional tectonic stress field, and dike intrusion (e.g., Curewitz & Karson, 1998; Umino et al., 2008) are all thought to create vertical and subvertical fractures and faults. Such processes are prominent in oceanic crust formed at slow spreading ridges (e.g., Blackman et al., 2006; Cann et al., 2015; Escartin & Lin, 1995), but they have also been documented at intermediate (e.g., Agar, 1990; Hayman & Karson, 2007; Karson, Klein, et al., 2002; Tartarotti et al., 1998), and fast and superfast (e.g., Bohnenstiehl & Carbotte, 2001; Le Saout et al., 2014; Soule et al., 2009; Tartarotti et al., 2009; Wright et al., 1995) spreading ridges. In fast spreading ridges such as the East Pacific Rise, fissuring and faulting have been inferred to be strongly linked to diking events that, at the ridge crest, may be as shallow as tens of meters and affect the morphology of the axial summit trough (e.g., Soule et al., 2009).

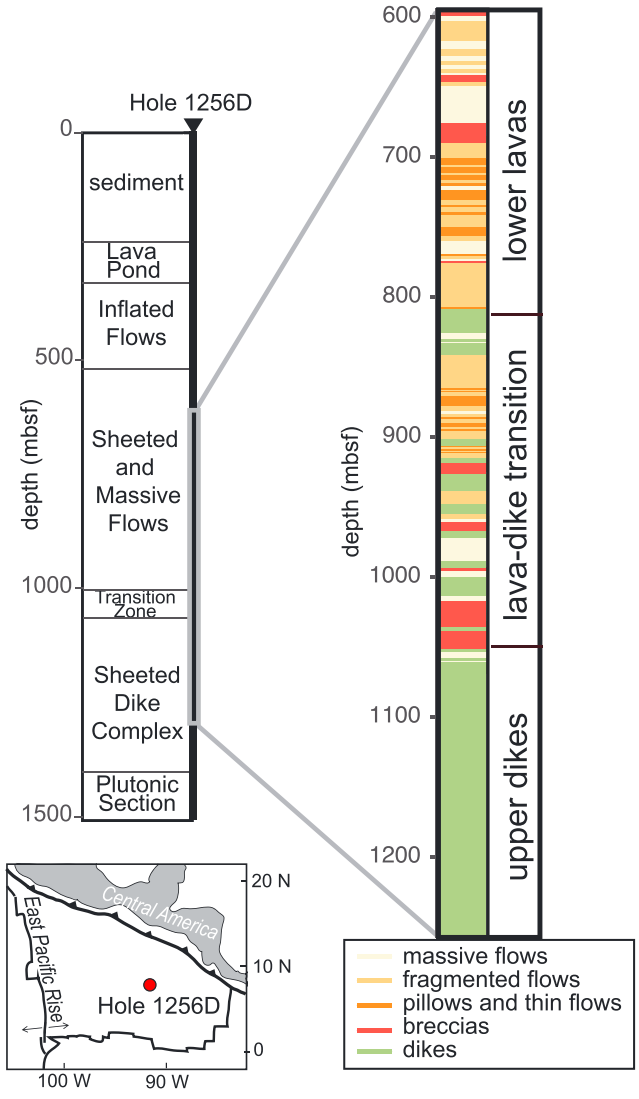

Figure 1. The studied interval within ODP-IODP Hole 1256D in the eastern Pacific Ocean. Generalized stratigraphy is from Teagle et al. (2006) and detailed lithostratigraphy is based on Tominaga et al. (2009).

In this study, we examine the permeability structure of the transition zone between the dikes and lavas. Ocean Drilling Program and Integrated Ocean Drilling Program (ODP-IODP) Hole 1256D provides an excellent site for testing the relationships between lithology, alteration, and permeability in crust formed at a superfast spreading rate, since it has been drilled in intact and in situ oceanic crust, where crustal stratigraphy has been built by magmatic (not tectonic) accretion. Examination of samples in the context of downhole measurements provides an opportunity to compare geophysical properties with interpretation of the geological origin of permeability in detail. Previous attempts to determine the permeability at ODP-IODP Hole 1256D have been limited to 25-m depth averages of hole bulk permeability calculated from electrical resistivity (Carlson, 2011) and laboratory measurements of 2.5-cm-diameter minicores without fractures (Gilbert & Bona, 2016). Using recovered cores, we examine the permeability structure of Hole 1256D at the centimeter to meter scale, a scale that is intermediate between most laboratory and field measurements of seafloor permeability (Fisher, 1998). We introduce a novel method for determining paleo-permeability based on the equivalent channel model of Walsh and Brace (1984) as applied by Morrow et al. (1994), which assumes that water moves through fractures in the crust in a way that is analogous to flow through a channel (e.g., Paterson, 1983). With this method, we address the locations of permeable zones recorded in recovered core, but also, for the first time, the orientation of crustal permeability from the lava-dike transition at Hole 1256D.

2. Geological Setting

ODP-IODP Hole 1256D (6°44.2′N, 091°56.1′W) has been drilled into 15-Myr-old crust that formed at the East Pacific Rise with a superfast full spreading rate of >200 mm/year (Wilson, 1996). Hole 1256D is located ~1150 km east of the present crest of the East Pacific Rise and ~530 km north of the Cocos Ridge (Figure 1). Hole 1256D has been deepened during four cruises, that is, ODP Leg 206 (Wilson et al., 2003), IODP Expeditions 309, 312, and 335 (Teagle et al., 2006, 2012) to reach a depth of 1,521.6 mbsf, making it at present the second deepest hole into oceanic basement. Hole 1256D is unique because gabbros have been reached by drilling for the first time in intact in situ ocean crust (Teagle et al., 2006; Wilson et al., 2006). Sediment thickness is ~250 m and the basement in Hole 1256D has been divided into six magmatic sections by Expedition 309/312 Scientists (2006a): *Lava Pond* (74 m thick), *Inflated Flows* (~183 m thick), *Sheet and Massive Flows* (~470 m thick), *Transition Zone* (~60 m thick), the *Sheeted Dike Complex* (~350 m thick), and *Plutonic Section* (Figure 1).

Given its structural setting, the lava-dike transition is expected to be characterized by some of the most permeable rocks encountered downhole in Hole 1256D. The *Transition Zone* at Hole 1256D, as formally defined during IODP Expedition 309 (Expedition 309/312 Scientists, 2006a), extends from ~1,004 to 1,061 mbsf (Figure 1), below the *Sheet and Massive Flows* and above *Sheeted Dike Complex*. The upper boundary of the *Transition Zone* at Hole 1256D was placed at 1,004.2 mbsf where the first occurrence of a subvertical intrusive contact (isolated dike) was identified in recovered core (Core 1256D-117R-1).

The *Transition Zone* also marks the boundary between low-temperature alteration above and hydrothermal (subgreenschist facies) alteration below (Figure 2). This alteration boundary extends from 981 to 1,027 mbsf (Teagle et al., 2006), which is at a shallower depth and partly overlaps the *Transition Zone*. The *Transition Zone* consists of intensely veined basaltic sheets and also includes a cataclastic unit in the upper part (Figure 2b) and mineralized volcanic breccias in the lower part (Figure 2c). In the cataclastic unit the igneous texture is

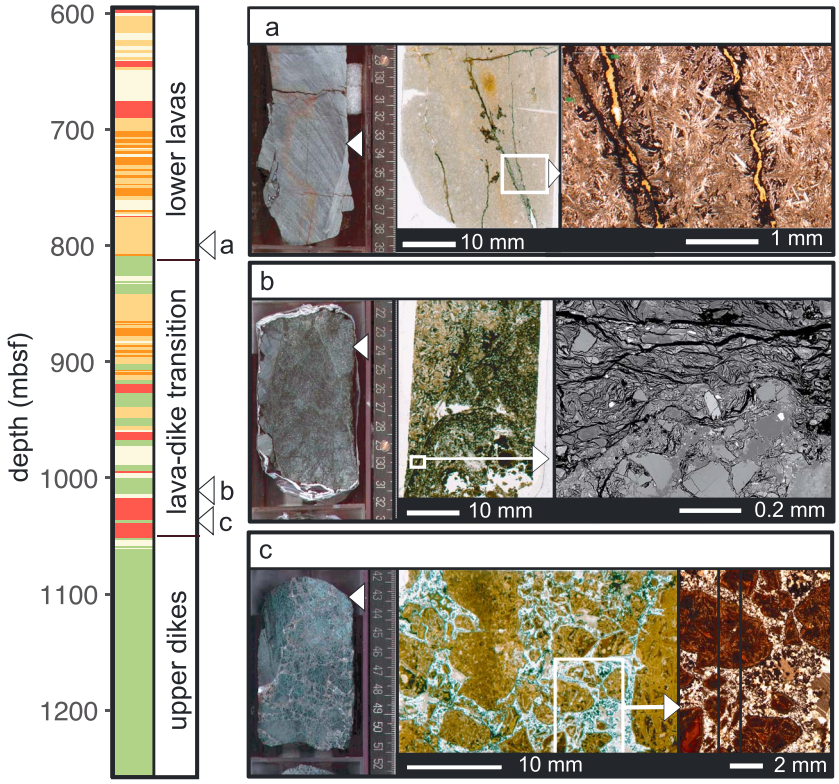

Figure 2. Core images, thin sections, and details within thin sections, summarizing the main structures and microstructures found in the studied interval at Hole 1256D. (a) Portion of Core 1256D-83R-1, 133–136 cm is representative of subvertical veins; thin section includes subvertical veins filled with clay minerals and opaque minerals. (b) Portion of Core 1256D-117R-1, 122–127 cm is representative of cataclasite: thin section and backscattered electron (BSE) image show the boundary between (top) cataclasite-rich in phyllosilicate minerals and (bottom) less brecciated host rock. (c) Portion of Core 1256D-122R-1, 41–44 cm shows the mineralized hyaloclastite breccia. Core photos and stratigraphic column from Teagle et al. (2006). Legend for detailed lithostratigraphy is in Figure 1.

no longer preserved and the rock is characterized by clasts of cryptocrystalline basalt or glass in a fine- to medium-grained basaltic breccia cut by an intensive network of thin chlorite-smectite veins (Teagle et al., 2006). The volcanic breccias comprise angular or subangular clasts of aphyric basalt or altered glass cemented by chalcedony, saponite, calcium carbonate, albite, anhydrite, and sulfides (Teagle et al., 2006). Smectite, mixed chlorite-smectite, Fe-oxyhydroxide, quartz, chalcedony, and calcite are common and hyaloclastic breccias host sulfides (mainly pyrite) with chalcedony, quartz, calcite, anhydrite, and minor amphibole cement (Figure 2).

The uppermost appearance of an isolated dike identified in borehole imaging by Tominaga et al. (2009) is at 815.95 mbsf. It is likely that fracturing and fluid circulation affected a crustal interval extending up to that appearance of the first dike from the *Sheeted Dikes* (which extend up to 1,065.7 mbsf according to Tominaga et al. (2009)), that is, a zone much thicker than the *Transition Zone* as originally defined by Teagle et al. (2006). To better constrain the downhole variability of structures and permeability in the lava-dike transition, the present study addresses a larger crustal interval chosen arbitrarily from 596.1 to 1,255.7 mbsf (i.e., from Core 1256D-51 to Core 1256D-170) that overlaps three units, for example, the lower *Sheet and Massive Flows,* the *Transition Zone,* and the upper *Sheeted Dike Complex* (Figure 1).

3. Methods and Data

Our overall approach is to synthesize core-based structural and alteration measurements and photos taken during ODP Leg 206 and IODP Expedition 309 (Teagle et al., 2006; Wilson et al., 2003) and then apply a channel model to calculate paleo-permeability.

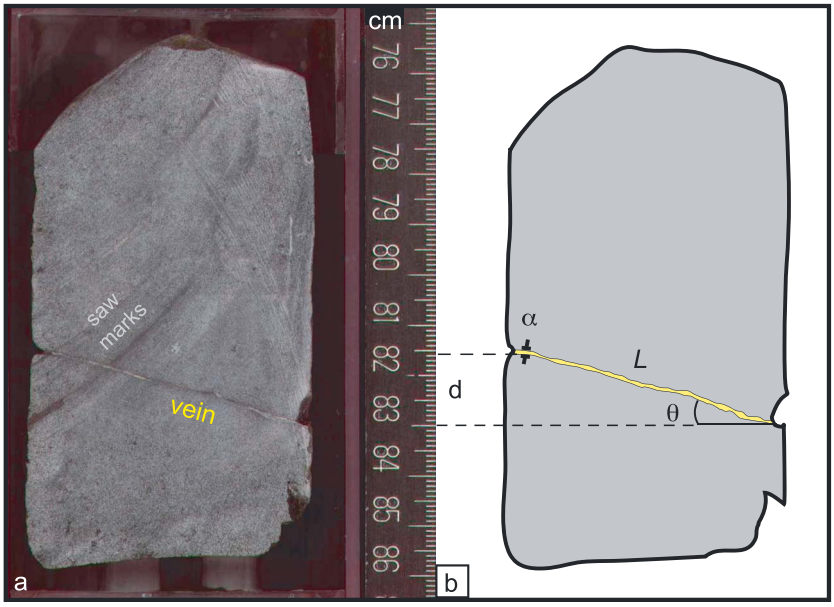

Figure 3. Example of an oriented core piece (up is at the top of the image) with one vein: (a) photo and (b) sketch. Recorded in the structural log are aperture (α), dip (θ), and the vertical distance (d) between the top and bottom of the vein. Vein length (L) is d*sin^{-1}(θ).

3.1. Core-Based Structural Data

We review the shipboard data from features which are potential conduits for fluid flow—past or present—reported in the Leg 206 and Expedition 309 Vein Log and Structural Log (Teagle et al., 2006; Wilson et al., 2003). We synthesize the logs into comprehensive databases by individual feature (Data Sets S1 and S2) and by piece (Data Sets S3 and S4). Data include measurements of the brittle structures such as the type of structure (e.g., open fracture, vein, shear vein, fault), length, aperture, filling material, and attitude, namely, the dip angle (see "Core description" in Expedition 309/312 Scientists, 2006b). The Structural Log details a variety of structures, including veins, breccias, joints, shear veins, faults, and intrusive dike contacts, and also includes dip information, but only within the vertically oriented pieces (i.e., not rubble or pieces otherwise too small to orient). The Structural Log omits structures with morphologies indicative of rock fracturing during cooling (i.e., veins with *Y*-shaped intersections and sinuous, steeply dipping veins intersected by radiating veins) and disk fractures that result from drilling since the regional stress field was the main interest during data collection. The Vein Log has the most comprehensive account of the number of veins and breccia intervals in all pieces, regardless of orientation or mechanism of formation. The Vein Log does not address orientation except to indicate vertical veins, where appropriate.

Measurements of the apertures of permeability conduits were recorded in the Vein Log and Structural Log by shipboard scientists to the nearest tenth of a millimeter, and lengths to the nearest centimeter. Although there some fractures have variable aperture (e.g., Figure 3), the average aperture was recorded in the Logs. These measurements are generally made by teams of two or more scientists, and in the case of Leg 206 and Expedition 309, several of the same scientists participated in both to further ensure consistency.

The faces of the cores, from which the structures were observed, were split at sea without knowing which direction pointed north. Care was taken to split cores orthogonal to dipping structural features so that such features were preserved relatively equally in both halves of the core (Teagle et al., 2006). Later core-log integration allowed for some limited references to geographic orientation (e.g., Fontana et al., 2010; Tominaga et al., 2009), but we did not geographically orient data. Dip angles are based on the assumption of a vertical drill hole (Teagle et al., 2006).

3.2. Paleo-Permeability Calculation

We calculate the original permeability or "paleo-permeability" (k_f) of each permeable feature using an equivalent channel model (e.g., Morrow et al., 1994; Paterson, 1983; Walsh & Brace, 1984) to represent each feature as a conduit:

$$k_f = \frac{h^2}{bF} \tag{1}$$

where b is a constant equal to 3 for cracks (Walsh & Brace, 1984). Hydraulic radius, h, is the ratio of conduit volume to surface area. For rectangular cross-section cracks,

$$h = \frac{\alpha L}{2(\alpha + L)} \tag{2}$$

where α is the crack aperture and L is the crack length observed in the core (Figure 3). Assuming $L >> \alpha$ for cracks, h is approximated as $\alpha/2$ (Patterson, 1983). Although a perfect orthogonal view of each fracture is unlikely in these cores, significant care was taken not to intersect fractures at high angles. Thus, we take the observed crack aperture, which is an apparent aperture, as a reasonable approximation of α. Also, the full length of each crack is almost always much larger than measured L, as shown by core-log integration studies (e.g., Fontana et al., 2010), but we are limited by the core view.

In equation (1), formation factor F is

$$F = \frac{T}{\phi^m} \tag{3}$$

Conduit tortuosity (T) is set to 1 because most observed permeable features were relatively straight (e.g., Figure 3). Pore fraction (ϕ) is the ratio of conduit area to core piece area. Piece area is the product of piece length and 5.8 cm, which is the average recovered core width reported by Teagle et al. (2006), although some pieces are irregular and smaller than the assumed 5.8-cm diameter. Conduit area is calculated as the product of α and conduit length, L (Figure 3). Conduit length in the Vein Log (Data Set S1) is approximated as the piece length for vertical veins. All other veins were given no dip direction in the Vein Log and as such, L is approximated as 5.8 cm (average piece width). Such a simplification may underestimate L—and thus k_f, but the effect is within the order of magnitude comparisons here and elsewhere (e.g., Fisher, 1998) relevant for interpreting permeability. In the Structural Log (Data Set S2), L is calculated as the product of d, the crack interval (bottom–top) and $\sin^{-1}\theta$, where θ is the dip angle (Figure 3). Note that d is recorded to the nearest centimeter curation depth. We use a cementation exponent, m, of 1 for open fracture permeability (Archie, 1942). We then combine equations (1)–(3) with the assumptions above to simplify

$$k_f = \frac{\alpha^2 \phi}{12} \tag{4}$$

The paleo-permeability of each feature, k_f, is determined individually using data in Data Set S1 (Vein Log) and Data Set S2 (Structural Log). Core pieces with a single permeable feature were assigned the associated k_f value. Core pieces with more than one permeable feature were assigned a paleo-permeability that was the sum of the k_f values from the piece (Data Sets S3 and S4).

Although α and ϕ are derived directly from the shipboard logs for veins, joints, and faults, these parameters are not readily available for the breccias. Before determining the paleo-permeability of each breccia with equation (4), we first divide the breccias into two groups: clast-supported breccias (Figure 4a) and matrix-supported breccias (Figure 4b), based on visual appearance of conduits for possible fluid flow (Data Set S1). We do not distinguish between types of breccia by origin, although most of the breccias at Hole 1256D are of hydrothermal origin (e.g., Figure 4b) and not fault breccias (Teagle et al., 2006). Second, we calculate α and ϕ based on measurements of breccia images. We approximate breccia α by counting and measuring the distances between clasts along horizontal cross sections of the images in Figure 4. The clast-supported breccia in Figure 4a has an average conduit aperture of 0.26 mm, with 3.5 conduits per centimeter. The matrix-supported breccia in Figure 4b has an average conduit aperture of 0.52 mm, also with 3.5 conduits per centimeter. We use α from the analyses of either Figure 4a or Figure 4b for each breccia, based on visual appearance. We assume breccia L equivalent to the thickness of each breccia interval

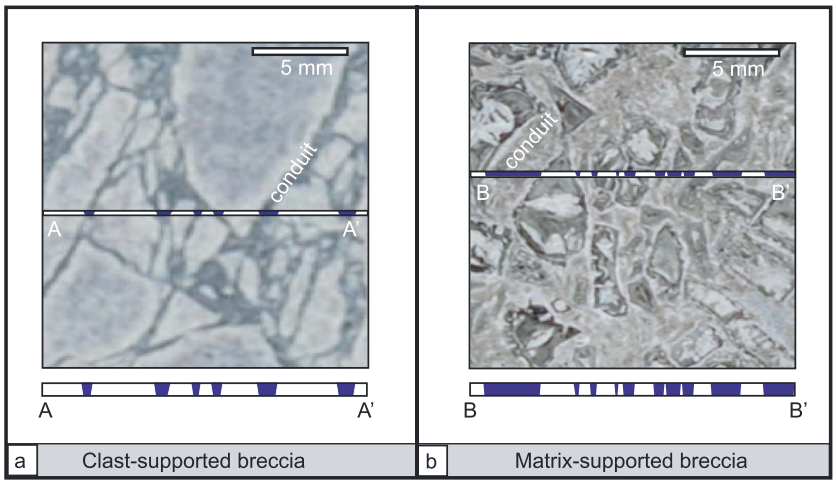

Figure 4. Close-up photos from two example breccias: (a) Core 1256D-161R-1, piece 3 and (b) Core 1256D-122R-2, piece 1 (International Ocean Discovery Program, 2015). All 87 breccias were either classified as (a) clast-supported or (b) matrix-supported based on visual similarity to these two examples. Individual conduit widths were measured across three horizontal lines of each of these two images. For example, one line is shown on each: A to A′ and B to B′; additional measurements (not shown) were made at the top and bottom of these images. The blue bars are the channels, and the white bars are the clasts. For simplicity, all clast-supported breccias are assumed to have an average conduit aperture of 0.26 mm and all matrix-supported breccias were assumed to have an average conduit aperture of 0.52 mm with 3.5 conduits per cm.

reported in the shipboard logs. Breccia ϕ (Data Set S1) is calculated from piece area and conduit area (from L and α), as for veins, joints, and faults.

3.3. Paleo-Permeability Uncertainties

The 0.05-mm uncertainty in shipboard aperture measurement results in higher uncertainties of k for lower α. For example, for α = 0.1 mm, k_f uncertainty is a factor of 4. In contrast, because conduits for flow within a breccia are relatively wide, α would have to be incorrectly determined as, for example, 30 mm instead of 15 mm for k_f uncertainty to be that large. The original conduit widths are also uncertain because of possible effects of infilling minerals expanding fractures and pressure closing fractures. We assume that original conduits were likely not any wider than those observed in the recovered cores, and therefore take the measured apertures as indicative of the maximum widths of the original fractures. In fact, due to mineral precipitation inside fractures, the original aperture could have been expanded, especially if repeated crack-seal have controlled such process.

4. Results

The permeable features (hereafter "fractures") observed in the investigated interval are veins (i.e., filled fractures, millimeter- to centimeter-thick) occurring as isolated veins or sets of parallel veins or vein networks, shear veins, open fractures, faults, Riedel-deformation bands, or intervals of cataclasites (<mm), incipient breccia, and hyaloclastic breccia hosting sulfide mineralization. We classify the fractures into three groups: veins, breccias, and other fractures (namely, joints and faults). In total, there are 6,682 veins, 87 breccia intervals, and 60 other fractures in the 659.6-m studied core interval. Below we summarize the paleo-permeabilities resulting from equations (1)–(4) by individual fracture (Data Set S1), individual oriented fracture (Data Set S2), piecewise for all veins and breccias (Data Set S3), and piecewise for oriented fractures only (Data Set S4). A large number of pieces in the studied interval (n = 815; 25%) have no observed fractures (i.e., no macroscopic vein, breccia, fault, or joint). Those pieces are assumed to be fairly intact and assigned a paleo-permeability of 10^{-20} m^2 based on results from unfractured basalt from Hole 1256D at in situ conditions by Gilbert and Bona (2016).

4.1. Veins

Veins are the dominant type of brittle structure in the upper basaltic crust at Hole 1256D and in the studied interval (i.e., 596.1–1,255.7 mbsf) they represent the most important potential permeable conduits for fluids.

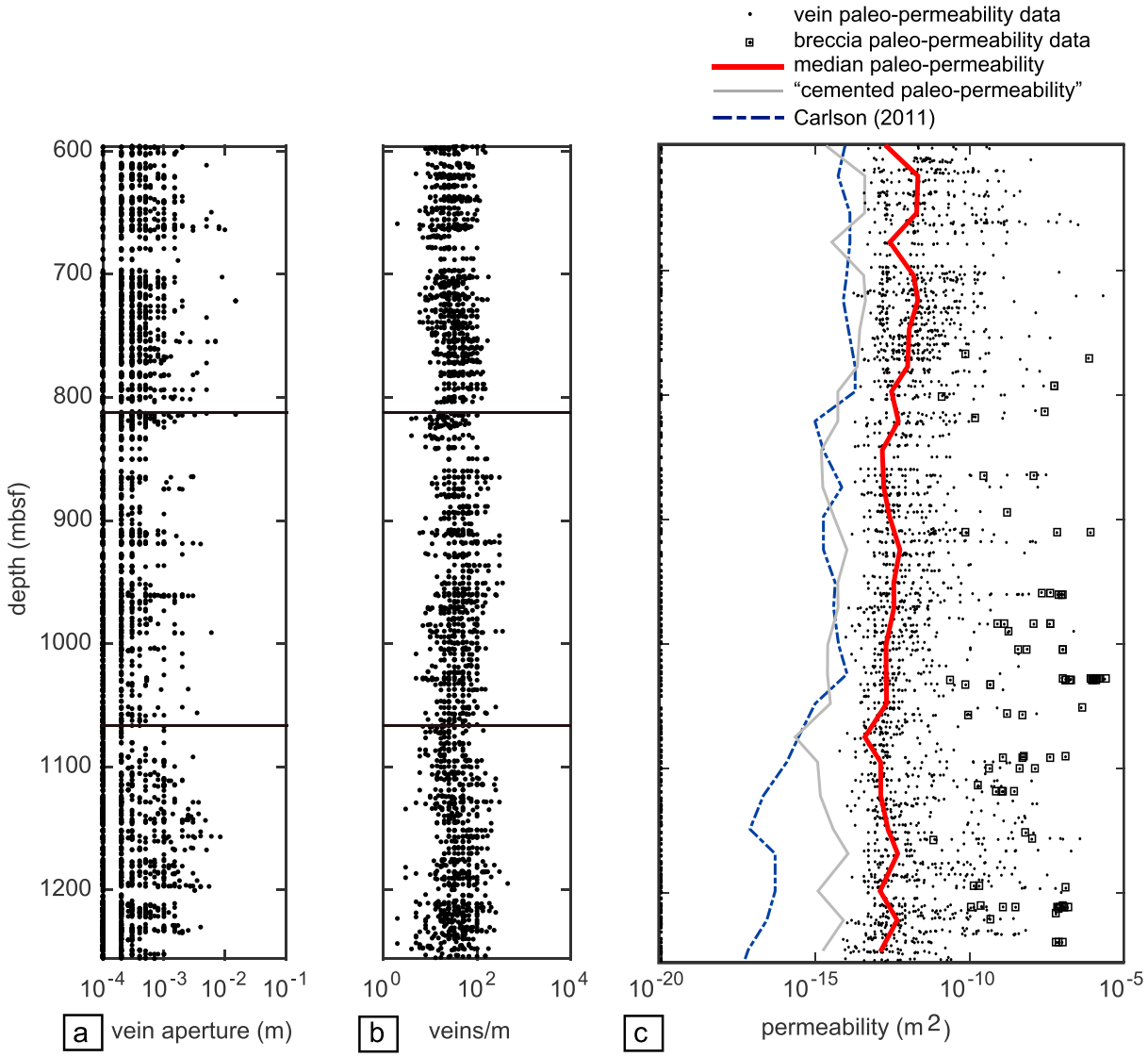

Figure 5. For the studied interval at Hole 1256D: (a) vein apertures and (b) veins per meter from the vein log (Data Set S3). (c) Paleo-permeability from piecewise vein log (dots; Data Set S3), including each paleo-permeability that includes breccia in the piece (boxes; Data Set S1). We compare Carlson (2011) data (blue dashed line, also every 25 m) to 25-m paleo-permeability medians (red solid line) and the "cemented paleo-permeability" profile (gray line) that results from considering the veins as cemented (m = 1.7 in equations (1)–(4)) instead of as open fractures (m = 1 in equations (1)–(4)).

Median vein aperture is 0.2 mm for the studied interval (Figure 5a). Within the studied cores, 82% of veins (n = 5,730) have aperture 0.1 to 0.4 mm and 3% of veins (n = 225) >1-mm aperture. The largest aperture vein is 15 mm (n = 5). Veins with small aperture were originally recorded as "<0.1 mm" (Teagle et al., 2006) and are here reported as 0.099 mm; these small veins are near the threshold of macroscopic visibility and represent 4% of veins between Cores 51 and 170 at Hole 1256D. There is an average of 31 veins per meter of recovered core (Table 1), with no significant trend with depth (Figure 5b).

4.2. Breccia

Within the studied interval, there are 87 breccias; 29 are matrix-supported and 58 are clast-supported (Data Set S1). Of the 87 breccia intervals recorded, 38 of them are noncontiguous with other breccias (9 matrix-supported and 29 clast-supported). Breccia comprises 4.7 m of the recovered cores in the studied interval, representing just 2% of core length. For pieces that are entirely matrix-supported breccia, paleo-porosity is 18% and paleo-permeability estimate is 1×10^{-9} m^2. For pieces that are entirely clast-supported breccia,

Table 1
Summary of Brittle Structures in the Studied Interval

	Lower lavas (596.1–811.3 mbsf)	Lava-dike transition (811.4–1064.9 mbsf)	Upper dikes (1065–1255.7 mbsf)	Studied interval (596.1–1255.7 mbsf)
Veins (N)	2386	2135	2343	6864
Breccias (N)	5	47	35	87
Vein and breccia density (N/m)	27	33	32	31
Recovered core length (m)	88.1	62.6	74.9	225.6
Recovery (%)	41	25	39	34

Note. Data are given in Data Set S1.

paleo-porosity is 9% and paleo-permeability estimate is 4×10^{-9} m^2 (Data Set S1). Although not a large fraction of the recovered cores, breccias represent important potential conduits for fluid flow and are included in the calculations of piece paleo-permeability (Data Set S3).

4.3. Oriented Fractures

Dip angles of all oriented structures indicate an overall downhole steepening of fractures (Figure 6). In the studied interval, there are fewer horizontal and subhorizontal (0–20°) structures (9%; n = 130) than vertical and subvertical (70–90°) structures (39%; n = 574). Horizontal structures are less dense and also have smaller apertures than vertical ones. Thus, due to both the density and aperture of fractures the paleo-permeability is largely oriented vertically and subvertically (Figure 6).

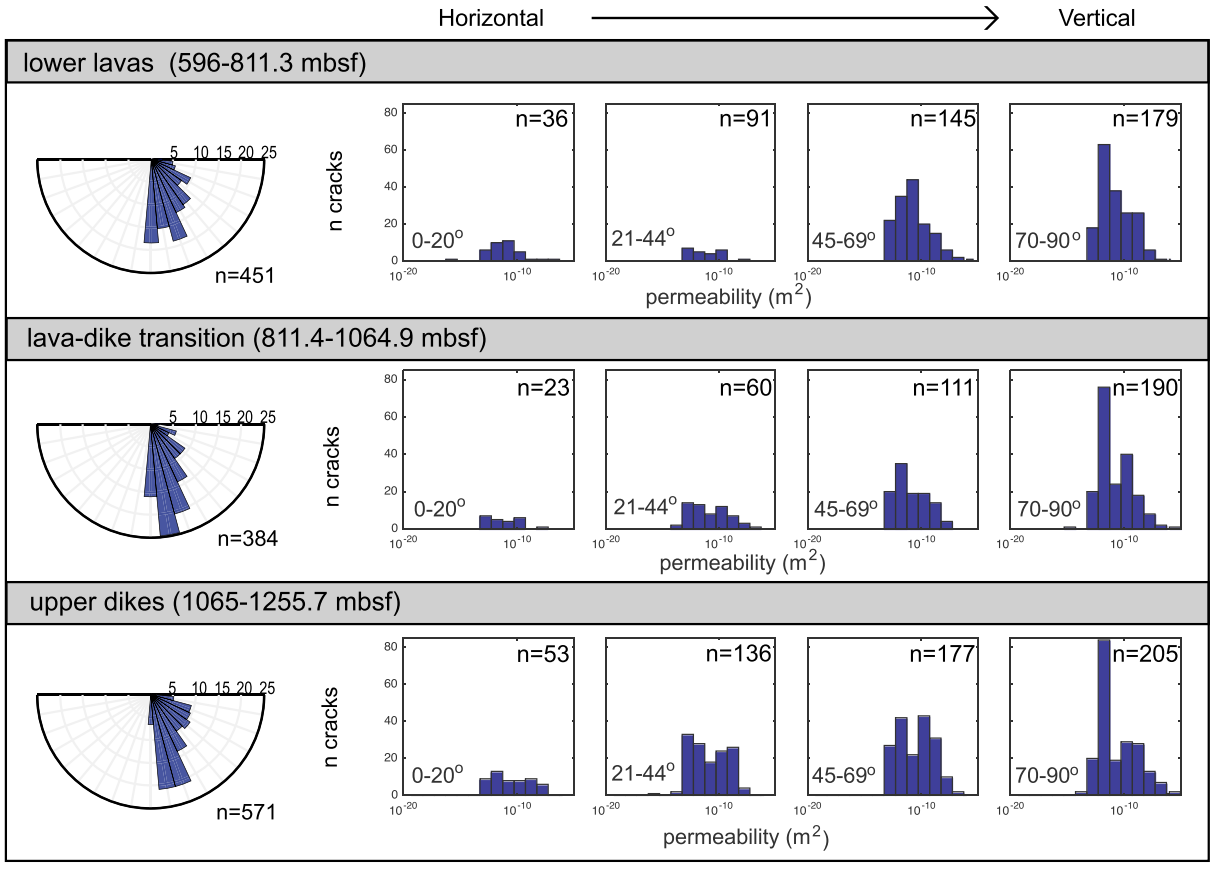

Figure 6. Distribution of oriented fractures within the studied interval. (left) Rose diagrams give overall distribution of fracture dips. Histograms show orientation of permeability for horizontal to subhorizontal (0–20°), intermediate shallow (21–44°), intermediate steep (45–69°), and subvertical to vertical (70–90°) fractures.

Of the 1,406 oriented features, most are veins (n = 1,346). Only 60 oriented brittle structures were identified as joints (n = 50) or faults (n = 10). Joints are primarily located in the *Sheeted Dikes* interval from 1,065.7 to 1,255.7 mbsf (n = 38). Faults in the studied interval were all found within the *Sheeted and Massive Flows* between 812.3 to 832.9 mbsf.

4.4. Paleo-Porosity and Paleo-Permeability

The maximum original porosity, or paleo-porosity, recorded by veins and breccias in the recovered cores from Hole 1256D varies significantly through the studied interval (Data Set S3). Median paleo-porosity of the lower lavas and lava-dike transition is 0.28 and 0.30%, respectively, with the difference not significantly different (two-tailed Wilcoxon rank-sum test, p = 0.72). Median paleo-porosity of the upper dikes is 0.17%, which is significantly lower than the lava-dike transition (one-tailed Wilcoxon rank-sum test, $p < 0.001$). However, those medians include a large number of pieces (n = 816 of 3,250) with no recorded brittle structures and thus using our method, have 0% paleo-porosity. Omitting the pieces with no observed brittle structures, median piece paleo-porosity is calculated as 0.38% (n = 2,434), with a minimum of 0.06% and a maximum of 42%. A total of 546 pieces have a paleo-porosity >1%, which represents a cumulative core length of 46.3 m. Only 92 pieces, mainly those with breccia, have paleo-porosity of >5%, which represents 6.3 m of core.

The maximum original permeability, or paleo-permeability, recorded by veins and breccias in the recovered cores from Hole 1256D, varies by more than 10 orders of magnitude (Data Set S3). Minimum and maximum paleo-permeabilities for pieces with observed brittle structures are 6×10^{-15} and 2×10^{-6} m^2, respectively, and the median is 1×10^{-14} m^2. For all pieces in the studied interval (n = 3,250), including those with no observed fractures, median paleo-permeability is 3×10^{-13} m^2 (Figure 5c). Paleo-permeability of recovered pieces decreases significantly with depth (Figure 5c). Median piece paleo-permeability is 1×10^{-12} m^2 in the lower lavas, 5×10^{-13} m^2 in the lava-dike transition, and 2×10^{-13} m^2 in the upper dikes (p = 0.0008 and $p < 0.001$, respectively, for one-tailed Wilcoxon rank-sum test).

5. Discussion

The crust at Hole 1256D has been significantly fractured (Teagle et al., 2006) and a record of that fracturing, albeit incomplete, is preserved in features observed in the recovered cores. We interpret our paleo-permeability results as a maximum original permeability of the crust immediately after fracturing, even though it is likely that those fractures were not open all at one time. Most of the fractures measured in the 15-Myr-old crust are sealed and record evidence of past hydrothermal fluid circulation (Alt et al., 2010). Below we discuss a revised definition of the lava-dike transition, the role of large fractures, and the importance of the orientation of paleo-permeability for understanding the history of fluid flow during crustal evolution.

5.1. Lava-Dike Transition

The studied interval was chosen to include cores from within, above, and below the transition from dikes to lavas in the crust at Hole 1256D. Tominaga et al. (2009) identified 28 isolated dikes above the *Sheeted Dikes* in wireline logs. In that study, the uppermost isolated dike is observed at 815.95-mbsf logging depth, which is located within recovered Core 1256D-85; the lowermost massive flow is at 1064-mbsf logging depth, which corresponds to Core 1256D-129. Because of depth uncertainty associated with core-log integration (Fontana et al., 2010; Tominaga et al., 2009), we define the lava-dike transition as an interval from 811.4 to 1,065.7 mbsf, which includes all of Core 1256D-85 and all of Core 1256D-129. Therefore, we suggest the full interval of lava-dike transition is ~254.3 m thick and extends nearly 200 m above the *Transition Zone* at Hole 1256D, although this may be an overestimation by as much as a few meters depending on the true depths of the cores within the cored intervals.

5.2. Large Fractures' Influence on Permeability

It has been previously hypothesized that a few large fractures may control fluid flow in the upper oceanic crust (e.g., Becker et al., 1994). Highly permeable features, which we define as individual veins, breccias, or other fractures with permeability $>10^{-9}$ m^2, dominate the paleo-permeability results reported here. Just 86 such features contribute >99% of the total permeability within the studied interval of the crust at Hole

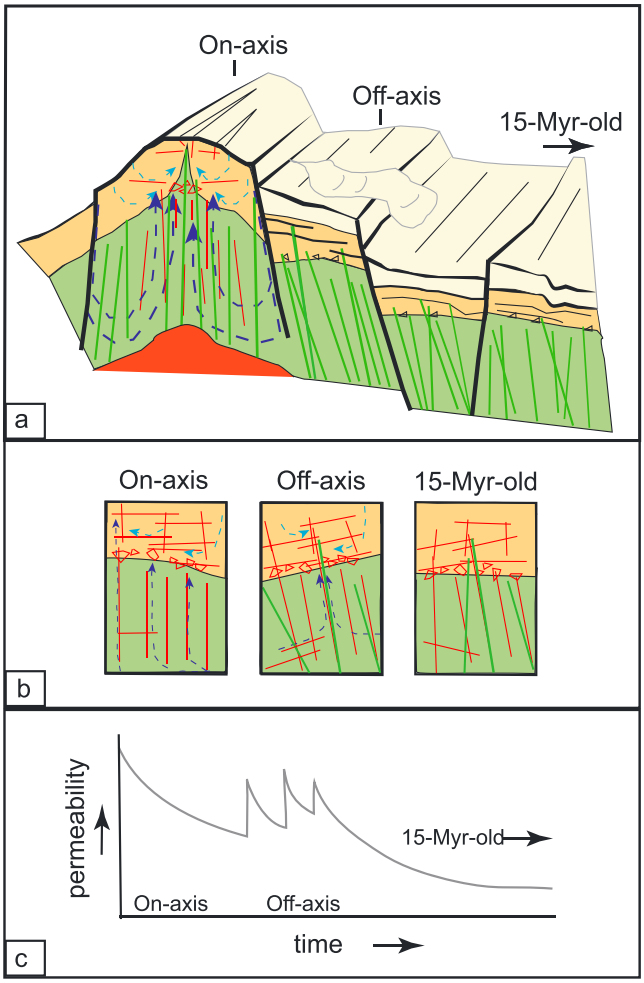

Figure 7. Evolution of permeability at the East Pacific rise: (a) cross-sectional diagram, (b) slices of the lava-dike transition, and (c) relative permeability model over time. In (b), the on-axis permeability structure is horizontal to subhorizontal in the lavas and vertical to subvertical in the dikes, with brecciation at the boundary between lavas and dikes due to upflow of hydrothermal fluids (blue arrows). Off-axis, the crust has been tilted by 10–20° away from the ridge axis, which tilts the permeability structure. New vertical and subvertical permeable pathways open from dikes intruding into the lower lavas. By 15 Myr, old pathways are sealed, and paleo-permeability structure is preserved by secondary minerals. Over time, in (c), the total permeability in the lava-dike transition gradually decreases due to gravity, faulting, and infilling. Initially, permeability is mainly controlled by horizontal contacts between flows, brecciated zones, and thermal contraction fractures. Permeability in the lava-dike transition dramatically increases with each diking event, and then fractures are sealed by low-temperature and hydrothermal minerals. Seawater continues to flow downward and laterally until the crust is hydrologically sealed. Colors in (a) and (b) are as in Figure 1 artwork.

1256D from the Vein Log (Data Set S1) and 59 such features contribute >99% of the oriented permeability from the Structural Log (Data Set S2). About half of the oriented highly permeable fractures are vertical or subvertical (n = 29). Few are horizontal or subhorizontal (n = 6). Within the lava-dike transition, no oriented highly permeable fractures are horizontal or subhorizontal. In the lava-dike transition and upper dikes, the highly permeable fractures have median dip angles of 85° and 75°, respectively.

Most of the veins measured in the studied interval of 596.1 to 1,255.7 mbsf are thin fractures with apertures of 0.3 mm or smaller (n = 5,797 or 83%). Of the oriented fractures, 56% are 0.3 mm or smaller (n = 785). At least 10^3 of these thin fractures are required to produce the increase in permeability created by a single >15-mm fracture, the largest fractures measured in the present study. Although smaller fractures may play important roles in chemical and heat exchange and influence the seismic properties of the crust (e.g., Carlson, 2014), it is the large fractures, which are undersampled by drilling, that have the potential to transmit tremendous volumes of water through the crust and thus control the overall hydrothermal circulation.

5.3. Orientation of Permeability

The average dip angle obtained from chilled margins and intrusive contacts in the *Sheeted Dikes* is steep: ~76° from shipboard measurements of core (Teagle et al., 2006) or ~79° from borehole images (Tominaga et al., 2009). Wireline imaging suggests that the crust dips slightly away from the paleo-spreading axis (~11° to the NE; Tominaga et al., 2009), suggesting the predominantly vertical and subvertical fractures reported here likely originated as vertical and subvertical features (Figure 7). Further, drilling produces known sampling bias: structures near-parallel to the drill hole are generally undersampled relative to structures that are near-perpendicular to the borehole (Martel, 1999). Because Hole 1256D is nearly vertical (Teagle et al., 2006), we are very likely underestimating the contributions of vertical features to paleo-permeability.

Throughout the studied interval, steeply dipping fractures dominate the crustal permeability structure. About half of the oriented fractures (49.7%; n = 187) in the lava-dike transition zone (811.4 to 1,065.7 mbsf) are vertical or subvertical (70–90°) and only 6% (n = 24) are horizontal or subhorizontal (0–20°). Within the lava-dike transition zone, median fracture dip angle is 69°. These vertical and subvertical fractures contribute significantly more to the permeability of the crust than horizontal and subhorizontal fractures (Figure 6). Specifically, vertical and subvertical fractures contribute 99.9% of permeability in lava-dike transition and 99.4% of permeability in the *Sheeted Dikes* (Figure 6). In the lower sections of the lavas (596.1–811.3 mbsf), 45–70° dipping structures contribute 69% of permeability and 70–90° structures contribute 26%. Structures with dip <45° contribute only 5% of the permeability of the lower lavas.

Fractures in the uppermost *Inflated Flows* are dominantly horizontal or subhorizontal (Tartarotti et al., 2009), in contrast to those in the lava-dike transition and upper *Sheeted Dikes*. Horizontal and subhorizontal features would be expected to originate during formation of lavas in the neovolcanic zone. These might later be rotated and further opened or closed during subsidence and thickening of the extrusive pile (Karson, Klein, et al., 2002). However, the prevalence of vertical fractures reaching into the lava-dike transition suggests diking events that reached into the accumulated lavas play an important role in determining the permeability structure of the oceanic crust as it ages.

5.4. Diking Events

A total of 86 dikes were identified by Tominaga et al. (2009) in Hole 1256D from 1,065 to 1,420 mbsf, within the *Sheeted Dikes*, most of them <1.0 m thick. With a modern dip of 11° away from the paleo-spreading center (Tominaga et al., 2009), this 355-m depth interval would span a lateral distance of 67.7 m, based on trigonometry. Assuming a superfast full spreading rate of 200 mm/year (Wilson, 1996), 67.7 m on one side of the ridge might represent roughly 677 years. If the dikes all formed at the spreading center, a diking recurrence interval of eight-year results—similar to the seven-year recurrence interval modeled at East Pacific Rise (150-mm/year full spreading rate) by Head III et al. (1996).

The variability of dike dip directions reported by Tominaga et al. (2009) supports the argument that diking into the lavas occurred across a large distance or, more likely, over thousands of years (Tominaga & Umino, 2010). The dikes in the *Sheeted Dikes* dip 64–90° in a fairly narrow range of dip directions between N and E, whereas the dikes in the lava-dike transition show significant variation in dip angle and direction (see Tominaga et al., 2009, Figure 11). The variable dip angle and direction of dikes within the lava-dike transition is consistent with observations at other locations including tectonic windows like the Blanco Transform Scarp and Hess Deep (Karson, Tivey, & Delaney, 2002; Varga et al., 2004).

Diking events into the lava-dike transition play an important role in the evolution of crustal permeability and the permeability structure of the crust that is preserved. With each diking event, the tensile stress field at the top of dikes could open or reopen fractures and faults that trigger the flow of fluids coming from the deeper portions of the ocean crust and/or from the seafloor and the topmost parts of the basement (Curewitz & Karson, 1998; Pollard & Segall, 1987; Rubin & Pollard, 1988; Soule et al., 2009). We can postulate that the lava-dike transition at Hole 1256D represents a stress field transition, from a deeper compressive to a shallower tensile stress field, as modeled by Curewitz and Karson (1998, and references therein). Diking is thus inferred to be the most efficient process that favors the opening of tensile fractures to channelize the upward flow of hydrothermal fluids. Dike intrusion at fast spreading ridges is inferred to be active at the ridge crest where dike tips may propagate to a depth as shallow as ~60 mbsf (e.g., Soule et al., 2009). Diking events at Hole 1256D are recorded in an aged crust (as old as 15 Myr) and may have reached such shallow depths but later buried by volcanism. More detailed studies on the structure and mineralogy of the *Sheeted Dike Complex* at Hole 1256D would be needed to unravel the diking evolution from the ridge crest to the present position and its relations to the crust permeability.

5.5. Evolution of Permeability in the Lava-Dike Transition

At Hole 1256D, Carlson (2011) found a bulk permeability of ~10^{-15} m^2 in the lava-dike transition and at nearby DSDP-ODP Hole 504B, packer injections tests of the 5.9-Myr crust indicate modern permeability in the lava-dike transition (~840–1,060 mbsf) of 10^{-16} to 10^{-15} m^2 (Becker, 1996). Our paleo-permeability results in the lava-dike transition are ~2 orders of magnitude higher than those estimates of modern permeability and we interpret the difference as sealing of the crust at the millimeter to centimeter scale.

Our median paleo-permeability profile from lava-dike transition veins, one per ~25 m from 800 to 1,050 mbsf (n = 11), mimics the modern downhole permeability pattern in Carlson (2011), with an offset. For comparison, we also include a "cemented paleo-permeability" profile using m = 1.7 for cemented fractures in equations (1)–(4), after Violay et al. (2010) and Roubinet et al. (2018). In the lava-dike transition, the paleo-permeability results are ~50 times higher than both the "cemented paleo-permeability" and the Carlson (2011) profile. The Carlson (2011) profile diverges in character significantly from our paleo-permeability profile at the top of the *Sheeted Dikes* (Figure 5c). The sharp decrease in permeability modeled by Carlson (2011) is largely controlled by the chosen model, which uses a porosity of 10% for the lavas and 1.2% for the dikes. Measurements of samples from Hole 1256D indicate porosity decreases at that boundary from 4% above to 2% below (Teagle et al., 2006). Our results also suggest a roughly 50% decrease in paleo-porosity at that boundary, at least not at the millimeter to meter scale represented in the recovered cores.

The 15-Myr-old crust at Hole 1256D is not thought to be hydrothermally active at present. After drilling, a temperature anomaly at ~850–1,000 mbsf, centered at 925 mbsf (Teagle et al., 2006, 2012), indicates that cold water may be entering the hole, but no warm water anomalies were located. From the same interval, in recovered cores, veins exhibit low-temperature oxidation down to 900–950 mbsf and saponite down to 1,050 mbsf (Harris et al., 2015). On the other hand, the mineralogy and isotope profiles in the lava-dike transition suggest

that this was a hydrothermally active zone where downwelling cold fluids mixed with upwelling hot discharge fluids (Alt et al., 2010; Harris et al., 2015). The transition is characterized by a greenschist to subgreenschist metamorphic overprint with evidence of hydrothermal alteration (Alt et al., 2010). Estimations of temperatures from secondary minerals at the lava-dike transition in Hole 1256D show a step in the thermal gradient at the base of the lava-dike transition (see Alt et al., 2010, Figure 13) coincident with chlorite as main phyllosilicate mineral and Mg-hornblende. The early minerals in veins and wall rock (i.e., clinopyroxene, amphiboles, chlorite, albite-oligoclase) give temperatures ~540–650 °C, which were successively replaced by retrograde lower temperature minerals, such as actinolite, albite, and smectite (Alt et al., 2010).

Alt et al. (2010) suggest that fluid flow through cores recovered from Hole 1256D occurred over a period of at least ~10,000 years. During this same period, diking events and lava flows continued construction of crust from the ridge axis to the axial summit (Tominaga & Umino, 2010). Before off-axis diking into lavas, permeability structure is mainly controlled by (mostly horizontal) contacts between flows or pillows, brecciated zones, and thermal contraction fractures. Each successive diking event locally increases vertical and subvertical permeability through fracturing of the crust. However, the lavas have significantly lower paleo-permeability than the lava-dike transition and *Sheeted Dikes,* and fewer vertical pathways (Figure 6), which might limit the upward migration of hydrothermal fluids. Associated hydrothermal fluids would be locally characterized by relatively elevated fluid pressure, creating a feedback to increase permeability. Microstructures of incipient breccias and of cataclasites record such events of weakening of the crust by elevated fluid pressure (Figure 2; Caine et al., 1996; Faulkner & Rutter, 2001; Umino et al., 2008).

5.6. Geophysical Evolution of the Lava-Dike Transition

During on-axis eruptions at fast and superfast spreading crust, the lava pile builds and initial reduction of porosity and permeability is primarily due to mechanical collapse of macroscopic (cm to m) drainbacks and cavities of what will become the lower lavas. Seismic layer 2A shifts upward as eruptions proceed and faulting and subsidence associated spreading (Karson, Klein, et al., 2002) further reduces the permeability and porosity of the lower lavas. As seawater and hydrothermal fluids circulate in open fractures, deposition of minerals significantly reduces the total water volume, or porosity, within the lower lavas. With each new dike that intrudes into the lower lavas as they move off-axis, permeability is temporarily increased (Figure 7c), as is porosity, which leads to a temporary decrease in local seismic velocity. Although the geophysical properties of the lava-dike transition likely never exceed the initial conditions of on-axis lavas, these off-axis dike intrusions lead to a more complex increase in seismic velocity with age than might be predicted by a gradual waning of eruption, faulting, and hydrothermal flow (Carlson, 1998; Christeson et al., 2007; Houtz & Ewing, 1976; Karson, 2002).

5.7. Advantages and Limitations of the Paleo-Permeability Method

The paleo-permeability method is a relatively straightforward way to estimate paleo-porosity and paleo-permeability in two dimensions at a variety of scales. The method has the advantage of addressing both total and directional paleo-permeability, where orientation information is available. In the absence of a CT scan, the paleo-permeability method allows us to estimate the maximum original permeability of a sample or core prior to crustal sealing by hydrothermal or other fluids. A limitation of the method is that the paleo-permeability estimates may represent only a very brief time before minerals begin to fill in fractures, especially for breccias of hydrothermal origin. The method also assumes all fractures were open at once, which is unlikely, and that the fractures did not widen as a result of mineral precipitation.

Data from cores provides a limited two-dimensional view of the ocean crust, in a fairly narrow (5.8 cm wide) swath. Although care was taken at sea to split the cores for an orthogonal view of fractures and we examined the three-dimensional geometry of breccia clasts in several perpendicular thin sections to confirm no significant anisotropy, the channel model assumes that measurements of aperture are made in a minimum cross-sectional view of the fluid conduit. Measurements at any other angle would artificially inflate the paleo-permeability.

Finally, the paleo-permeability method as applied here is also limited to the features which are visible to the naked eye and recovered by drilling. About 25% of the recovered pieces appear to be unfractured, with no visible structures. We assumed that these pieces have a low permeability, on the order of ~10^{-20} m^2 at in situ conditions, but there may be an order of magnitude or more variability in micropaleo-permeability (Gilbert &

Bona, 2016). Perhaps most importantly, recovery of core at Hole 1256D was incomplete, 34% within the studied interval. The results reported here are based on that record, which is not only incomplete, but also likely biased toward the more coherent rocks. It is therefore likely that some important zones of high permeability at Hole 1256D were missing from the recovered core and, as a result, omitted from this study.

6. Conclusions

In fractured basaltic crust, which is characteristic of seafloor formed at a spreading ridge, high-permeability zones are distributed at variable depth intervals and do not conform to a strict trend with depth. At Hole 1256D, the permeability structure is strongly controlled by fracture attitude and aperture. The lava-dike transition represents a crucial boundary for examining the permeability structure because it represents a change in the stress field due to intrusive diking. The depth interval of 811.4–1,065.7 mbsf in Hole 1256D, more than 1,004.2–1,060.9 mbsf (i.e., the original *Transition Zone*) is marked by a change in permeable structure attitude, from subvertical (at depth) to more gently dipping above. While some vertical fractures are likely due to the effect of cooling and contraction of lava, the significant increase in vertical fractures with depth is coincident with and likely strongly controlled by dike intrusion. The vertical permeability created by dike intrusion following initial emplacement of lavas enables continued upflow of hydrothermal fluids. Evidence of significant hydrothermal flow is recorded in the veins preserved in the crust recovered from Hole 1256D and studied by others (e.g., Alt et al., 2010; Harris et al., 2015). The original *Transition Zone* and the lower part of the *Sheet and Massive Flows*, a zone we term the lava-dike transition, thus marks a boundary layer between crustal sections characterized by a different stress field, permeability regime, and metamorphic imprint.

Acknowledgments
This research used data accessible at http://iodp.tamu.edu/database/ and samples provided by the International Ocean Discovery Program (IODP). The authors acknowledge the many scientists and crew members aboard ODP Leg 206 and IODP Expedition 309 for their efforts to collect the samples and data and E.R. Olson for feedback on an earlier version of this manuscript. Rick Walker, two anonymous reviewers, and the Associate Editor provided useful feedback for improving this manuscript. L.A.G. is grateful to the Earth & Planetary Sciences Department at the University California Santa Cruz and the Geology Department at the University of Otago for their hospitality during her sabbatical leave when much of this work was completed. Funding was provided by the Sperry Fund and Geosciences Department at Williams College. The authors declare no conflicts of interest.

References

Agar, S. M. (1990). Fracture evolution in the upper ocean crust: Evidence from DSDP Hole 504B. In R. J. Knipe & E. H. Rutter (Eds.), *Deformation Mechanism, Rheology and Tectonics* (Vol. 54, pp. 41–50). London: Geological Society, London, Special Publications.

Alt, J. C., Laverne, C., Coggon, R. M., Teagle, D. A. H., Banerjee, N. R., Morgan, S., et al. (2010). Subsurface structure of a submarine hydrothermal system in ocean crust formed at the East Pacific Rise, ODP/IODP Site 1256. *Geochemistry, Geophysics, Geosystems*, *11*, Q10010. https://doi.org/10.1029/2010GC003144

Anderson, R. N., Honnorez, J., Becker, K., et al. (1985). *Initial Reports Deep Sea Drilling Project* (Vol. 83). Washington, DC: U.S. Government Printing office.

Archie, G. E. (1942). The electrical resistivity log as an aid in determining some reservoir characteristics. *Trans. Am. Inst. Mech. Eng.*, *146*, 54–62.

Becker, K. (1996). In J. C. Alt, H. Kinoshita, L. B. Stokking, & P. J. Michael (Eds.), *Permeability Measurements in Hole 896A and Implications for the Lateral Variability of Upper Crustal Permeability at Sites 504 and 896*, *Proc. ODP, Sci. Results, 148* (pp. 353–363). College Station, TX: Ocean Drilling Program. https://doi.org/10.2973/odp.proc.sr.148.135.1996

Becker, K., Davis, E., Spiess, F., & deMoustier, C. (2004). Temperature and video logs from the upper oceanic crust, Holes 504B and 896A, Costa Rica rift flank: Implications for the permeability of upper oceanic crust. *Earth and Planetary Science Letters*, *222*(3-4), 881–896. https://doi.org/10.1016/j. epsl.2004.03.033

Becker, K., Morin, R. H., & Davis, E. E. (1994). Permeabilities in the Middle Valley hydrothermal system measured with packer and flow meter experiments. In M. J. Mottl, E. E. Davis, A. T. Fisher, & J. F. Slack (Eds.). *Proceeding of the Ocean Drilling Program, Scientific Results*, *139*, 613–626.

Blackman, D. K., Ildefonse, B., John, B. E., Ohara, Y., Miller, D. J., MacLeod, C. J., & the expedition 304/305 scientists (2006). *Proceedings of the Integrated Ocean Drilling Program*, (Vol. 304/305), doi:https://doi.org/10.2204/iodp.proc.304305.2006). College Station, Texas: ocean drilling program.

Bohnenstiehl, D. W. R., & Carbotte, S. M. (2001). Faulting patterns near 19°30′S on the East Pacific rise: Fault formation and growth at a superfast spreading center. *Geochemistry, Geophysics, Geosystems*, *2*(9). https://doi.org/10.1029/2001GC000156

Caine, J. S., Evans, J. P., & Forster, C. B. (1996). Fault zone architecture and permeability structure. *Geology*, *24*(11), 1025–1028. https://doi.org/10.1130/0091-7613(1996)024<1025:FZAAPS>2.3.CO;2

Cann, J. R., Smith, D. K., Escartin, J., & Schouten, H. (2015). Tectonic evolution of 200 km of mid-Atlantic ridge over 10 million years: Interplay of volcanism and faulting. *Geochemistry, Geophysics, Geosystems*, *16*, 2303–2321. https://doi.org/10.1002/2015GC005797

Carlson, R. L. (1998). Seismic velocities in the uppermost oceanic crust: Age dependence and the fate of layer 2A. *Journal of Geophysical Research*, *103*(B4), 7069–7077. https://doi.org/10.1029/97JB03577

Carlson, R. L. (2010). How crack porosity and shape control seismic velocities in the upper oceanic crust: Modeling downhole logs from Holes 504B and 1256D. *Geochemistry, Geophysics, Geosystems*, *11*, Q04007. https://doi.org/10.1029/2009GC002955

Carlson, R. L. (2011). The effect of hydrothermal alteration on the seismic structure of the upper oceanic crust: Evidence from holes 504B and 1256D. *Geochemistry, Geophysics, Geosystems*, *12*, Q09013. https://doi.org/10.1029/2011GC003624

Carlson, R. L. (2014). The effects of alteration and porosity on seismic velocities in oceanic basalts and diabases. *Geochemistry, Geophysics, Geosystems*, *15*, 4589–4598. https://doi.org/10.1002/2014GC005537

Christeson, G. L., Karson, J. A., & McIntosh, K. D. (2010). Mapping of seismic layer 2A/2B boundary above the sheeted dike unit at intermediate-spreading crust exposed near the Blanko transform. *Geochemistry, Geophysics, Geosystems*, *11*, Q03015. https://doi.org/10.1029/2009GC002864

Christeson, G. L., McIntosh, K. D., & Karson, J. A. (2007). Inconsistent correlation of seismic layer 2a and lava layer thickness in oceanic crust. *Nature*, *445*(7126), 418–421. https://doi.org/10.1038/nature05517

Christeson, G. L., Morgan, J. V., & Warner, M. R. (2012). Shallow oceanic crust: Full waveform tomographic images of the seismic layer 2A/2B boundary. *Journal of Geophysical Research*, *117*, B05101. https://doi.org/10.1029/2011JB008972

Curewitz, D., & Karson, J. A. (1998). Geological consequences of dike intrusion at mid-ocean ridge spreading centers. In W. R. Buck, P. T. Delaney, J. A. Karson, & Y. Lagabrielle (Eds.), *Faulting and Magmatism at Mid-Ocean Ridges, Geophysical Monograph Series* (Vol. 106, pp. 117–136). Washington, DC: American Geophysical Union.

Escartin, J., & Lin, J. (1995). Ridge offsets, normal faulting, and gravity anomalies of slow slpreading ridges. *Journal of Geophysical Research*, *100*(B4), 6163–6177. https://doi.org/10.1029/94JB03267

Expedition 309/312 Scientists (2006a). Site 1256. In D. A. H. Teagle, J. C. Alt, S. Umino, S. Miyashita, N. R. Banerjee, D. S. Wilson, & the Expedition 309/312 Scientists (Eds.), *Proceedings of the Integrated Ocean Drilling Program* (Vol.309/312, pp. 1–549). Washington, DC, Integrated Ocean Drilling Program Management International, Inc. https://doi.org/10.2204/iodp.proc.309312.103.2006

Expedition 309/312 Scientists (2006b). Methods. In D. A. H. Teagle, J. C. Alt, S. Umino, S. Miyashita, N. R. Banerjee, D. S. Wilson, & the Expedition 309/312 Scientists (Eds.), *Proceedings of the Integrated Ocean Drilling Program* (Vol. 309/312, pp. 1–70). Washington, DC, Integrated Ocean Drilling Program Management International, Inc. https://doi.org/10.2204/iodp.proc.309312.102.2006

Faulkner, D. R., & Rutter, E. H. (2001). Can the maintenance of overpressured fluids in large strike-slip fault zones explain their apparent weakness? *Geology*, *29*(6), 503–506. https://doi.org/10.1130/0091-7613(2001)029<0503:CTMOOF>2.0.CO;2

Fisher, A. T. (1998). Permeability within basaltic oceanic crust. *Reviews of Geophysics*, *36*(2), 143–182. https://doi.org/10.1029/97RG02916

Fontana, E., Iturrino, G. J., & Tartarotti, P. (2010). Depth-shifting and orientation of core data using a core-log integration approach: A case study from ODP-IODP Hole 1256D. *Tectonophysics*, *494*(1-2), 85–100. https://doi.org/10.1016/j.tecto.2010.09.006

Fox, P. J., Schreiber, E., & Peterson, J. J. (1973). The geology of the oceanic crust: Compressional wave velocities of oceanic rocks. *Journal of Geophysical Research*, *78*(23), 5155–5172. https://doi.org/10.1029/JB078i023p05155

Gilbert, L. A., & Bona, M. L. (2016). Permeability of oceanic crustal rock samples from IODP Hole 1256D. *Geochemistry, Geophysics, Geosystystems.*, *17*, 3825–3832. https://doi.org/10.1002/2016GC006467

Gilbert, L. A., & Salisbury, M. H. (2011). Oceanic crustal velocities from laboratory and logging measurements of Integrated Ocean drilling program Hole 1256D. *Geochemistry, Geophysics, Geosystystems*, *12*, Q09001. https://doi.org/10.1029/2011GC003750

Gillis, K. M. (1995). Controls on hydrothermal alteration in a section of fast-spreading oceanic crust. *Earth and Planetary Science Letters*, *134*(3-4), 473–489. https://doi.org/10.1016/0012-821X(95)00137-2

Harris, M., Coggon, R. M., Smith-Duque, C. E., Cooper, M. J., Milton, J. A., & Teagle, D. A. H. (2015). Channelling of hydrothermal fluids during the accretion and evolution of the upper oceanic crust: Sr isotope evidence from ODP Hole 1256D. *Earth and Planetary Science Letters*, *416*, 56–66. https://doi.org/10.1016/j.epsl.2015.01.042

Hayman, N. W., & Karson, J. A. (2007). Faults and damage zones in fast-spread crust exposed on the north wall of the Hess deep rift: Conduits and seals in seafloor hydrothermal systems. *Geochemistry, Geophysics, Geosystystems*, *8*, Q10002. https://doi.org/10.1029/2007GC001623

Head, J. W. III, Wilson, L., & Smith, D. K. (1996). Mid-ocean ridge eruptive vent morphology and substructure: Evidence for dike widths, eruption rates, and evolution of eruptions and axial volcanic ridges. *Journal of Geophysical Research*, *101*(B12), 28265–28280. https://doi.org/10.1029/96JB02275

Honnorez, J., Alt, J. C., Honnorez-Guerstein, B.-M., Laverne, C., Muehlenbachs, K., Ruiz, J., & Saltzman, E. (1985). Stockwork-like sulfide mineralization in young oceanic crust: Deep Sea drilling project Hole 504B. In R. N. Anderson, J. Honnorez, K. Becker, et al. (Eds.), *Initial Reports Deep Sea Drilling Project* (Vol. 83, pp. 263–282). Washington, DC: U.S. Government Printing office.

Hooft, E. E. E., Schouten, H., & Detrick, R. S. (1996). Constraining crustal emplacement processes from the variation of seismic layer 2A thickness at the East Pacific rise. *Earth and Planetary Science Letters*, *142*(3-4), 289–309. https://doi.org/10.1016/0012-821X(96)00101-X

Houtz, R., & Ewing, J. (1976). Upper crustal structure as a function of plate age. *Journal of Geophysical Research*, *81*(14), 2490–2498. https://doi.org/10.1029/JB081i014p02490

International Ocean Discovery Program (2015). Janus data (Exp 1–312). http://iodp.tamu.edu/janusweb/links/links_all.shtml. Accessed 9 November 2017.

Karson, J. A. (2002). Geologic structure of the uppermost oceanic crust created at fast- to intermediate-rate spreading centers. *Annual Review of Earth and Planetary Sciences*, *30*(1), 347–384. https://doi.org/10.1146/annurev.earth.30.091201.141132

Karson, J. A., Klein, E. M., Hurst, S. D., Lee, C. E., Rivizzigno, P. A., Curewitz, D., et al. (2002). Structure of uppermost fast-spread oceanic crust exposed at the Hess deep rift: Implications for subaxial processes at the East Pacific rise. *Geochemistry, Geophysics, Geosystystems*, *3*(1), 1002. https://doi.org/10.1029/2001GC000155

Karson, J. A., Tivey, M. A., & Delaney, J. R. (2002). Internal structure of uppermost oceanic crust along the western Blanco transform scarp: Implications for subaxial accretion and deformation at the Juan de Fuca ridge. *Journal of Geophysical Research*, *107*(B9), 2181. https://doi.org/10.1029/2000JB000051

Le Saout, M., Deschamps, A., Soule, S. A., & Gente, P. (2014). Segmentation and eruptive activity along the East Pacific rise at 16°N, in relation with the nearby mathematician hotspot. *Geochemistry, Geophysics, Geosystems*, *15*, 4380–4399. https://doi.org/10.1002/2014GC005560

Lister, C. R. B. (1974). On the penetration of water into hot rock. *Geophysical Journal of the Royal Astronomical Society*, *39*(3), 465–509. https://doi.org/10.1111/j.1365-246X.1974.tb05468.x

Martel, S. J. (1999). Analysis of fracture orientation data from boreholes. *Environmental & Engineering Geoscience*, *5*(2), 213–233.

Morrow, C., Lockner, D., Hickman, S., Rusanov, M., & Röckel, T. (1994). Effects of lithology and depth on the permeability of core samples from the kola and KTB drill holes. *Journal of Geophysical Research*, *99*(B4), 7263–7274. https://doi.org/10.1029/93JB03458

Paterson, M. S. (1983). The equivalent channel model for permeability and resistivity in fluid-saturated rock—A re-appraisal. *Mechanics of Materials*, *2*(4), 345–352. https://doi.org/10.1016/0167-6636(83)90025-X

Pezard, P., Ayadi, M., Revil, A., Bronner, G., & Wilkens, R. (1997). Detailed structure of an ocean normal fault: A multiscalar approach at DSDP/ODP site 504. *Geophysical Research Letters*, *24*(3), 337–340. https://doi.org/10.1029/96GL03618

Pollard, D. D., & Segall, P. (1987). Theoretical displacements and stresses near fractures in rock: With applications to faults, joints, veins, dikes, and solution surfaces. In B. K. Atkinson (Ed.), *Fracture Mechanics of Rocks* (pp. 277–349). London, England: Academic Press.

Roubinet, D., Irving, J., & Pezard, P. A. (2018). Relating topological and electrical properties of fractured porous media: Insights into the characterization of rock fracturing. *Minerals*, *8*(1), 14. https://doi.org/10.3390/min8010014

Rowland, J. V., & Sibson, R. H. (2004). Structural controls on hydrothermal flow in a segmented rift system, Taupo volcanic zone, New Zealand. *Geofluids*, *4*(4), 259–283. https://doi.org/10.1111/j.1468-8123.2004.00091.x

Rubin, A. M., & Pollard, D. D. (1988). Dike-induced faulting in rift zones of Iceland and afar. *Geology*, *16*(5), 413–417. https://doi.org/10.1130/0091-7613(1988)016<0413:DIFIRZ>2.3.CO;2

Seher, T., Crawford, W., Singh, S., & Cannat, M. (2010). Seismic layer 2A variations in the lucky strike segment at the Mid-Atlantic Ridge from reflection measurements. *Journal of Geophysical Research*, *115*, B07107. https://doi.org/10.1029/2009JB006783

Soule, S. A., Escartín, J., & Fornari, D. J. (2009). A record of eruption and intrusion at a fast spreading ridge axis: Axial summit trough of the East Pacific Rise at 9–10°N. *Geochemistry, Geophysics, Geosystems*, *10*, Q10T07. https://doi.org/10.1029/2008GC002354

Tartarotti, P., Ayadi, M., Pezard, P. A., Laverne, C., & De Larouzière, F. F. (1998). Multi scalar structure at DSDP/ODP site 504, Costa Rica rift, II: Fracturing and alteration. An integrated study from core, downhole measurements and borehole wall images. In P. K. Harvey & M. A. Lovell (Eds.), *Core-Log Integration* (Vol. 136, pp. 391–412). London: Geological Society of London Special Publication.

Tartarotti, P., Fontana, E., & Crispini, L. (2009). Deformation pattern in a massive ponded lava flow at ODP-IODP Site 1256: A core and log approach. *Geochemistry, Geophysics, Geosystems*, *01*, Q05O17. https://doi.org/10.1029/2008GC002346

Teagle, D. A. H., Alt, J. C., Umino, S., Miyashita, S., Banerjee, N. R., Wilson, D. S., & the Expedition 309/312 Scientists (2006). *Proceeding of the Integrated Ocean Drilling Program* (Vol. 309/312). Washington, DC: Integrated Ocean Drilling Program Management International, Inc. https://doi.org/10.2204/iodp.proc.309312.2006

Teagle, D. A. H., Ildefonse, B., Blum, P., & the Expedition 335 Scientists (2012). *Proceeding of the Integrated Ocean Drilling Program* (Vol. 335). Tokyo: Integrated Ocean Drilling Program Management International, Inc. https://doi.org/10.2204/iodp.proc.335.2012

Tominaga, M., Teagle, D. A. H., Alt, J. C., & Umino, S. (2009). Determination of the volcanostratigraphy of oceanic crust formed at superfast spreading ridge: Electrofacies analyses of ODP/IODP Hole 1256D. *Geochemistry, Geophysics, Geosystystems*, *10*, Q01003. https://doi.org/10.1029/2008GC002143

Tominaga, M., & Umino, S. (2010). Lava deposition history in ODP Hole 1256D: Insights from log-based volcanostratigraphy. *Geochemistry, Geophysics, Geosystystems*, *11*, Q05003. https://doi.org/10.1029/2009GC002933

Tsang, C.-F., & Neretnieks, I. (1998). Flow channeling in heterogenous fractured rocks. *Reviews of Geophysics*, *36*(2), 275–298. https://doi.org/10.1029/97RG03319

Umino, S., Crispini, L., Tartarotti, P., Teagle, D. A. H., Alt, J. C., Miyashita, S., & Banerjee, N. R. (2008). Origin of the sheeted dike complex at superfast spread East Pacific Rise revealed by deep ocean crust drilling at Ocean Drilling Program Hole 1256D. *Geochemistry, Geophysics, Geosystems*, *9*, Q06O08. https://doi.org/10.1029/2007GC001760

Varga, R. J., Karson, J. A., & Gee, J. S. (2004). Paleomagnetic constraints on deformation models for uppermost oceanic crust exposed at the Hess deep rift: Implications for axial processes at the East Pacific rise. *Journal of Geophysical Research*, *109*, B02104. https://doi.org/10.1029/2003JB002486

Violay, M., Pezard, P. A., Ildefonse, B., Belghoul, A., & Laverne, C. (2010). Petrophysical properties of the root zone of the sheeted dikes in the ocean crust: A case study from Hole ODP/IODP 1256D, Eastern Equatorial Pacific. *Tectonophysics*, *493*(1-2), 139–152. https://doi.org/10.1016/j.tecto.2010.07.013

Walsh, J. B., & Brace, W. F. (1984). The effect of pressure on porosity and the transport properties of rock. *Journal of Geophysical Research*, *89*(B11), 9425–9431. https://doi.org/10.1029/JB089iB11p09425

Wilkens, R. H., Fryer, G. J., & Karsten, J. (1991). Evolution of porosity and seismic structure of upper oceanic crust: Importance of aspect ratios. *Journal of Geophysical Research*, *96*(B11), 17,981–17,995. https://doi.org/10.1029/91JB01454

Wilson, D. S. (1996). Fastest known spreading on the Miocene Cocos-Pacific plate boundary. *Geophysical Research Letters*, *23*(21), 3003–3006. https://doi.org/10.1029/96GL02893

Wilson, D. S., Teagle, D. A. H., Acton, G. D., et al. (2003). *Proceedings of the Ocean Drilling Program, Initial Reports, (Online)* (Vol. 206). College Station, TX: Ocean Drill. Program. https://doi.org/10.2973/odp.proc.ir.206.2003

Wilson, D. S., Teagle, D. A. H., Alt, J. C., Banerjee, N. R., Umino, S., Miyashita, S., et al. (2006). Drilling to gabbro in Intact Ocean crust. *Science*, *312*(5776), 1016–1020. https://doi.org/10.1126/science.1126090

Wright, D. J., Haymon, R. M., & Fornari, D. J. (1995). Crustal fissuring and its relationship to magmatic and hydrothermal processes on the East Pacific Rise crest (9°12′–54′N). *Journal of Geophysical Research*, *100*, 6097–6120. https://doi.org/10.1029/94JB02876